Tuning Methods for Classical SISO PID
Magnetic Levitation Controllers via Analytic Models

Nathan P. PETERSEN[a] and Eric L. SEVERSON[a]

[a] *University of Wisconsin–Madison, Madison, WI, USA. Email: nathan.petersen@wisc.edu, eric.severson@wisc.edu*

Abstract

Stable operation of magnetically levitated systems requires feedback control. This paper studies tuning methodologies for the popular stabilizing PID controller which generates force/current references for the inner control loop. The pole placement method and frequency design loop shaping methods are compared in terms of their required tuning rules. Since the control system has five parameters, the tuning process is under constrained since the system only has two parameters: rotor mass and displacement unstable stiffness. Therefore, system performance objective metrics are defined and a case study multi-objective optimization is performed to find Pareto optimal tunings. Six tuning regions are identified and the salient characteristics are given and transformed into tuning rules. For example, it is found that high phase margin does not necessarily translate to robust control, nor a highly damped system response. Future magnetic levitation control designers can use the practical rules herein as a guide for creating robust and high-performance feedback PID controllers for magnetic levitation.

Keywords: magnetic levitation, tuning, PID control, frequency design, pole placement

1 Introduction

Magnetic levitation has been applied to rotating machinery where either active magnetic bearings (AMBs) or bearingless motors (BMs) are used, see Fig. 1. Both AMBs and BMs can be viewed as generic force actuators and made to accurately create a desired force. To achieve stable levitation, motion controllers use displacement measurements to compute a force command which the AMBs/BMs produce. There are potential complexities to the motion control algorithm, e.g., speed-dependent bearing stiffness/damping to handle the dynamics of flexible rotors, co-location issues between the force production and sensor planes, and handling imbalance in the rotor assembly. While complexities may abound for real-world systems, this paper is devoted to understanding the tuning of classical PID controllers for the linear magnetic levitation mechanical plant with mass m and unstable displacement stiffness (positive number) k_δ. While the core theoretic tuning concepts are known in the literature, the goal of this paper is to present a practical and systematic methodology to implement this theory in real systems.
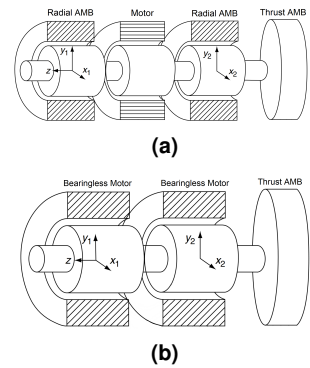
Fig. 1: *Non-contact motor with: (a) AMBs, (b) BMs. (Chiba et al. 2005)*

2 Control Structure

Figure 2 shows control of AMBs/BMs where an inner force (current) regulation loop produces a force command F_c^* with high bandwidth. The outer motion control loop is used to stabilize the system by measuring rotor displacement δ and computing the force reference F_c^* for the inner loop. The starred signals (e.g., δ^*) denote references and i is the current, F_{dis} is the disturbance force, and k_f is the bearing current stiffness constant. The motion controller is denoted $G_c(s)$, the current (force) regulation loop dynamics are modeled as $G_{CR}(s)$, and the magnetic levitation plant is denoted $G_p(s)$. These transfer functions are assumed to be in the form:

$$G_c(s) = K_P + \frac{K_I}{s} + K_D s \left(\frac{\omega_D}{s + \omega_D} \right) \qquad G_{CR}(s) = \frac{\omega_{ci}}{s + \omega_{ci}} \qquad G_p(s) = \frac{1}{ms^2 - k_\delta} \qquad (1)$$
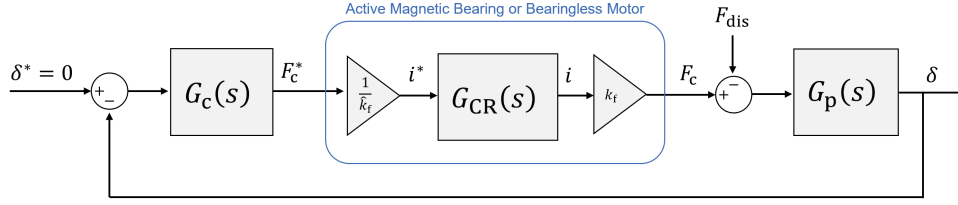
Fig. 2: Single DOF magnetic levitation control structure showing the AMB or BM as the force actuator.

The controller $G_c(s)$ is classical PID with an additional low-pass filter (pole) inline with the derivative term to limit the effects of sensor noise. The current regulator $G_{CR}(s)$ is modeled as a first-order low-pass filter (pole) at bandwidth ω_{ci}. The plant $G_p(s)$ is modeled as a mass-spring system with destabilizing spring stiffness; both AMBs and BMs behave according to this model for small displacements from center (Chiba et al. 2005, Maslen et al. 2009). The plant $G_p(s)$ can also be written as two poles where one is in the right-half plane (i.e., unstable) and is located at unstable pole frequency $\omega_0 = \sqrt{k_\delta/m}$. The value of $\omega_0/2\pi$ is typically 20-50 Hz.

3 Tuning Methods

There are several studies published related to controller tuning in magnetic levitation systems. Tuning for PID and PD controllers is investigated in (Bleuler et al. 1994, Anantachaisilp et al. 2012); linear quadratic regulation (LQR) is studied in (Brunet & Rioland 1990, Yoon et al. 2012); automated controller design and tuning using μ-synthesis is investigated in (Sawicki & Maslen 2008). These prior studies give several frameworks for reasoning through controller tuning, however, these studies do not give simple analytical equations and "rules of thumb" that control designers can use when approaching controller gain selection for system bring-up. In this paper, two practical tuning methodologies broadly applicable to SISO magnetic levitation controllers are investigated: (i) pole placement and (ii) frequency domain loop shaping.

Referring to Fig. 2 and (1), a complete controller tuning can then be described as $x \in \mathbb{R}^5$ where $x = [K_P, K_I, K_D, \omega_D, \omega_{ci}]$ and K_P, K_I, and K_D are the PID gains; ω_D is the derivative-term (d-term) filter bandwidth; and ω_{ci} is the inner current regulation bandwidth. In practice, $\omega_{ci} < \omega_{ci,max}$ and $\omega_D < \omega_{D,max}$. The filter bandwidths must be high enough so as to not impede stable controller operation.

3.1 Pole Placement Method

It is well known that the closed-loop poles of a system directly impact the system behavior, such as determining bandwidths, settling times, and transient oscillations. Since this system is controllable, linear systems theory states that the closed-loop poles can be placed arbitrarily through gain selection. The task of the control designer is then to select appropriate locations for the poles such that the final system behaves as desired. The following steps are required to algebraically solve the pole-placement problem. First, the open-loop $\mathrm{OL}(s)$ and closed-loop $\mathrm{CL}(s)$ transfer functions of the 1-DOF control system can be derived as:

$$\mathrm{OL}(s) = \frac{k_f}{\hat{k}_f} G_c(s) G_{CR}(s) G_p(s), \qquad \mathrm{CL}(s) = \frac{\delta(s)}{\delta^*(s)} = \frac{\mathrm{OL}(s)}{1 + \mathrm{OL}(s)} = \frac{A_2 s^2 + A_1 s + A_0}{s^5 + B_4 s^4 + B_3 s^3 + B_2 s^2 + B_1 s + B_0} \quad (2)$$

A generic polynomial $P(s)$ of equal order to the characteristic polynomial (denominator of $\mathrm{CL}(s)$) is defined:

$$P(s) = (s-a)(s-b)(s-c)(s-d)(s-e) = s^5 + P_4 s^4 + P_3 s^3 + P_2 s^2 + P_1 s + P_0 \quad (3)$$

The coefficients of the characteristic polynomial and $P(s)$ are equated: $P_k = B_k$ for $k = 0 \dots 4$. This forms five equations with five unknowns. The five unknowns are the controller gains $x = [K_P, K_I, K_D, \omega_D, \omega_{ci}]$ which can be found by solving the system of equations, i.e., $x = f(a, b, c, d, e)$. Due to the fifth-order system, it is recommended to use a symbolic math package to solve for x.

3.2 Frequency Design Method

The frequency design method is an alternative way of reasoning about the tuning of the PID controller. By studying the open-loop transfer function $OL(s)$ and viewing the controller $G_c(s)$ in pole-zero form, Bode plot analysis can be readily used, i.e., metrics like gain/phase margin and gain/phase crossover frequency. The PID controller from (1) can be rewritten in pole-zero form as (4) where there are two zeros at frequencies ω_{z1} and ω_{z2}, one pole at frequency ω_D, one pole at the origin, and gain K_o. To tune the control system using the frequency design method, the control designer must specify five metrics: phase margin ϕ_{PM}, gain crossover frequency (i.e., controller bandwidth) ω_c, one of the two zeros ω_{z1}, pole ω_D, and current regulator bandwidth ω_{ci}. Based on these inputs, the second zero ω_{z2} is computed to achieve the desired phase margin ϕ_{PM} and the gain K_o is computed such that $|OL(j\omega_c)| = 1$, see the expressions from (5).

$$
G_{c,\mathrm{zpk}}(s) = K_o \frac{(1 + \frac{s}{\omega_{z1}})(1 + \frac{s}{\omega_{z2}})}{s(1 + \frac{s}{\omega_D})} \text{ where } K_P = \left(\frac{1}{\omega_{z1}} + \frac{1}{\omega_{z2}} - \frac{1}{\omega_D} \right) K_o, \ K_I = K_o, \ K_D = \frac{K_o}{\omega_{z1}\omega_{z2}} - \frac{K_P}{\omega_D} \quad (4)
$$

$$
\omega_{z2} = \frac{\omega_c}{\tan\left(\phi_{PM} + \frac{\pi}{2} - \mathrm{atan}(\frac{\omega_c}{\omega_{z1}}) + \mathrm{atan}(\frac{\omega_c}{\omega_D}) + \mathrm{atan}(\frac{\omega_c}{\omega_{ci}}) \right)}, \quad K_o = \frac{1}{\left. |G_c(j\omega_c)| \right|_{K_o=1} |G_{CR}(j\omega_c)| |G_p(j\omega_c)|} \quad (5)
$$

3.3 Required Tuning Rules

The process of using either the pole placement method or the frequency design method simply requires evaluating closed-form expressions to solve for the controller gains. However, both methods require the control designer to specify five tuning "rules of thumb" to fully constrain the math. The remainder of this paper investigates how to reason about "good" tuning rules.

4 Tuning Rules for PID Controllers

This section explores trade-offs in system performance between tunings with the goal of presenting guidelines for selecting tuning rules which give optimal controller performance for both the pole placement and frequency design methods. Numerical methods combined with an evolutionary algorithm are used to search the magnetic levitation controller tuning design space to identify Pareto optimal tuning approaches.

4.1 Controller Optimization Formulation

The controller performance is evaluated with three objectives (to maximize):

- O_1: phase margin ϕ_{PM}—generally desired in control systems and helps ensure stability even when unmodeled dynamics are present, for example, eddy currents which limit achievable force bandwidth.
- O_2: allowable parameter error ($\pm$) in m, k_δ, or k_f before closed-loop instability—all real-world systems have some degree of uncertainty in plant parameters which the controller must tolerate.
- O_3: $\frac{1}{\|\delta(s)/F_{\mathrm{dis}}(s)\|_\infty}$, i.e., the lowest dynamic stiffness value over all frequencies—since magnetic levitation systems only respond to force disturbances, this term denotes the effective controller effort.

Three constraints are enforced: $O_2 > 10\%$, $\omega_{ci} \leq \omega_{ci,\max} = 2\pi \times 1500$ Hz, $\omega_D \leq \omega_{D,\max} = 2\pi \times 800$ Hz. The plant studied has $m = 1$ kg and $\omega_0/2\pi = 50$ Hz. The optimization procedure uses a population-based multi-objective evolutionary genetic algorithm. Each individual in the population maps to one set of tuning gains. The optimization free variables are the s-plane location of the five closed-loop poles from Section 3.1. Three optimization cases are performed: (1) all real poles, (2) three real poles with one pair of complex conjugate poles, and (3) one real pole with two pairs of complex conjugate poles. The genetic algorithm was run until convergence, i.e., the Pareto front remained static over multiple generations. Multiple optimization runs were conducted with random initial populations to ensure global optimal solutions.

(a)

(b)

(c)
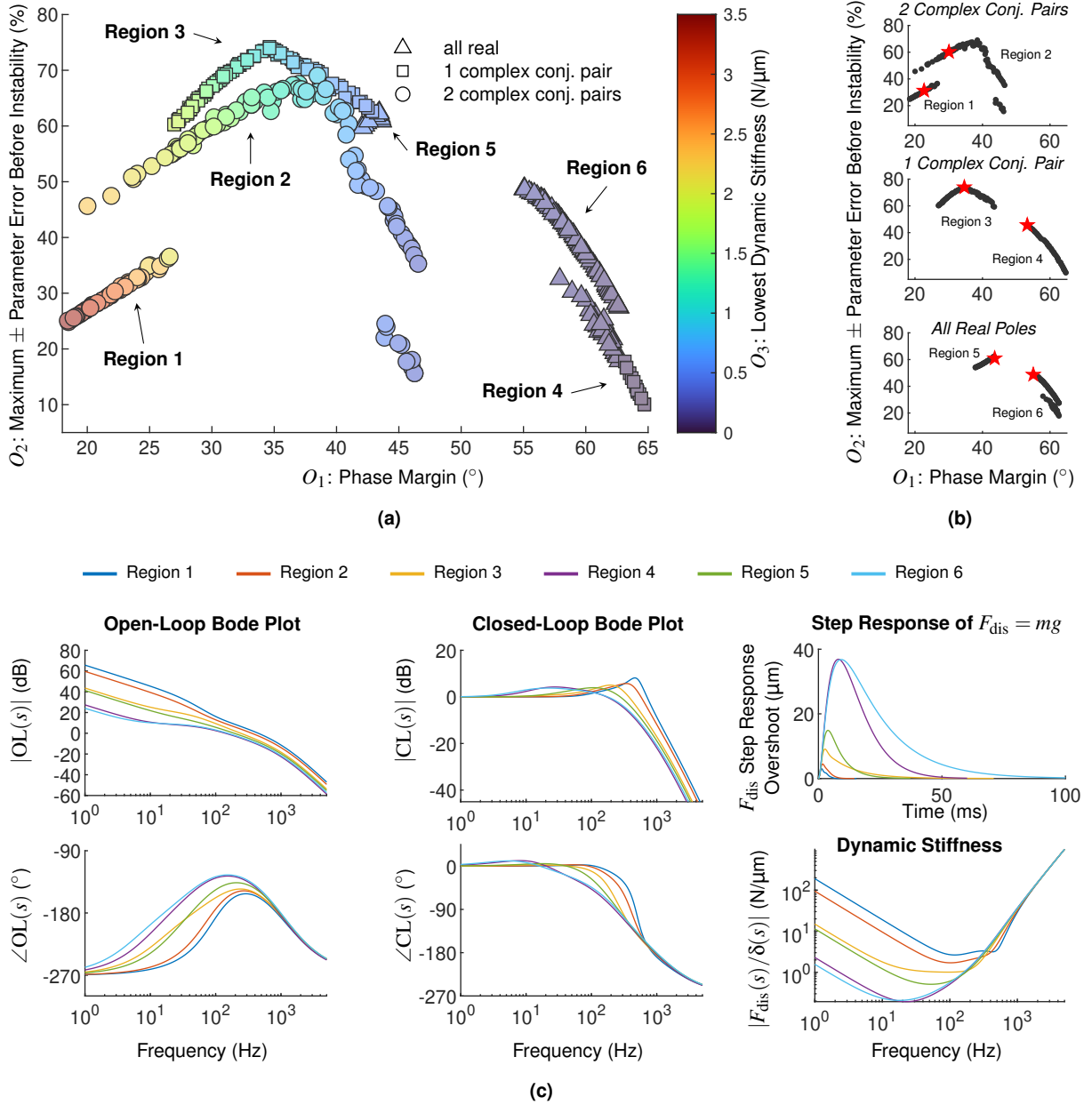
Fig. 3: *Optimization Pareto fronts. Each marker denotes one controller tuning set. (a) Combined global Pareto front; (b) Individual Pareto fronts. (c) System response for the marked tunings from (b).*

Region	$\omega_c/2\pi$ (Hz)	ϕ_{PM} (°)	$\omega_{z1}/2\pi$ (Hz)	$\omega_{z2}/2\pi$ (Hz)	$\omega_D/2\pi$ (Hz)	$\omega_{ci}/2\pi$ (Hz)	$-a/2\pi$ (Hz)	$-b/2\pi$ (Hz)	$-c/2\pi$ (Hz)	$-d/2\pi$ (Hz)	$-e/2\pi$ (Hz)
1	449	23	74.2 + j57.4	$\omega_{z1}^{\dagger}$	769	1386	1714.8	132.1 + j483.1	$b^{\dagger}$	87.6 + j65.1	$e^{\dagger}$
2	358	30	66.6 + j39.0	$\omega_{z1}^{\dagger}$	781	1432	1700.0	172.5 + j382.3	$b^{\dagger}$	84.4 + j43.1	$e^{\dagger}$
3	242	35	13.6	114.6	794	1393	1588.1	299.3	142.2 + j195.7	$c^{\dagger}$	15.0
4	141	53	9.0	41.5	797	1213	1388.9	375.4	200.7	22.4 + j5.9	$d^{\dagger}$
5	192	44	22.4	64.2	800	1412	1584.5	234.2	233.0	131.2	28.8
6	152	55	5.5	42.8	798	1368	1526.1	349.7	247.0	33.6	9.7

Table 1: *Summary of selected Pareto optimal tunings denoted in Fig. 3b.*
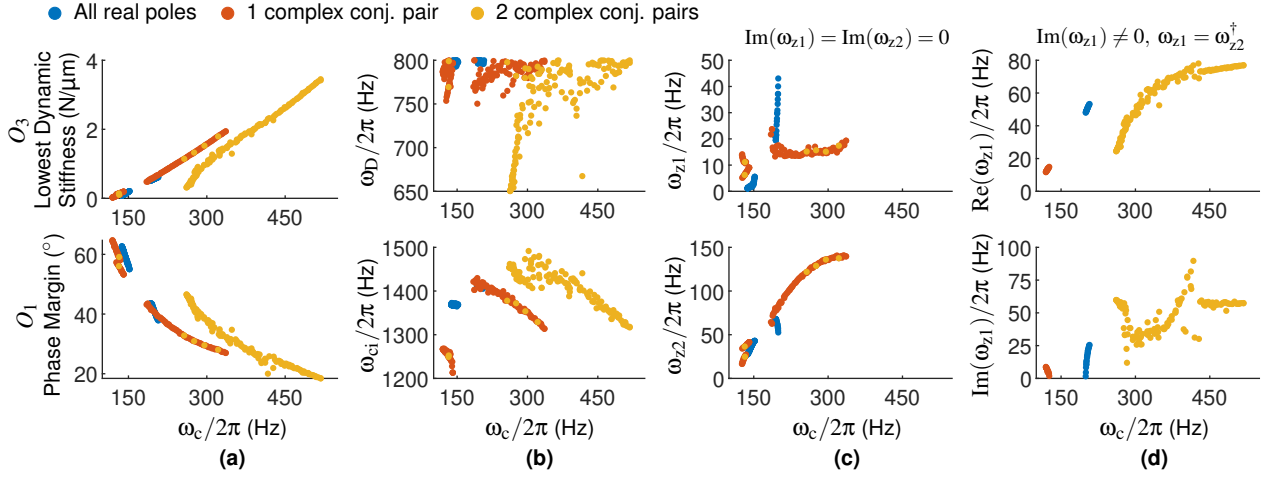
Fig. 4: *Trends in Pareto optimal tunings vs. PID controller bandwidth, i.e., gain crossover frequency* ω_c.

4.2 Optimization Results

Fig. 3 shows the Pareto fronts from the controller tuning optimization studies. Fig. 3a shows the global Pareto front while Fig. 3b shows the Pareto fronts from each case. There are six regions labeled on the Pareto fronts based on the natural segmentation of the results, each resulting in different system performance. The starred points from Fig. 3b are evaluated and the response is shown in Fig. 3c and Table 1. Fig. 4 shows trends in control metrics across Pareto optimal tunings compared to the PID controller bandwidth ω_c. Fig. 4a shows the objectives O_1 and O_3. It is seen that the control bandwidth ω_c is proportional to the lowest dynamic stiffness, and for a given ω_c, the case of two complex conj. pole pairs has worse stiffness compared to only one complex conj. pole pair. However, with two complex conj. pole pairs, the controller can be tuned to bandwidth/stiffness values far beyond what is possible with only one complex conj. pole pair. The phase margin ϕ_{PM} degrades with increasing control bandwidth ω_c. Fig. 4b shows the filter bandwidths for the d-term pole ω_D and current regulator ω_{ci}. The optimization has pushed the d-term filter bandwidth to its limit for many cases, however, this is not true for the current regulation bandwidth. The controller zero (ω_{z1}, ω_{z2}) placement is given where the pure real zeros are shown in Fig. 4c and the complex conj. zeros are shown in Fig. 4d.

4.3 Controller Tuning Regions

The characterization of each of the six tuning regions is compared to give tuning recommendations such as the form of the closed-loop poles and the placement of the PID controller zeros. In this section, the closed-loop poles $[a, b, c, d, e]$ are assumed to be sorted by increasing real part, i.e., $\Re(a) \leq \Re(b) \leq \Re(c)$ etc. For all tunings, the fastest pole a is purely real and is spaced far from the next pole b, i.e., $|\Re(a)| \gg |\Re(b)|$. The placement of a is set according to the current regulation bandwidth limit $\omega_{ci,max}$, however, $|a| \neq \omega_{ci,max}$ since the closed-loop and open-loop poles are not equal.

4.3.1 Regions 1 and 2—two complex conjugate closed-loop pole pairs

Regions 1 and 2 are characterized by the controller zeros—in the pole-zero form from (4)—being complex conjugates, i.e., $\omega_{z1} = \omega_{z1,r} + j\omega_{z1,i}$ and $\omega_{z2} = \omega_{z1}^\dagger$. The frequency design method tuning equations presented in Section 3.2 do not handle complex conjugate controller zeros, however, the pole placement method from Section 3.1 inherently does. For all tunings from both Regions 1 and 2, the slower pair of complex conjugate poles (i.e., d and e) are located close to the complex conjugate controller zeros, thus achieving partial pole/zero cancellation. By doing this, the system response has no noticeable oscillations, even though the closed-loop poles consist of two pairs of complex conjugates, and the faster pair has no zero cancellation effect.

4.3.2   Regions 3 and 4—one complex conjugate closed-loop pole pair

Region 3 is characterized by the closed-loop poles c and d being the complex conjugate pair, i.e., the slowest pole e is purely real. In other words, as sorted, $c = c_r + jc_i$ and $d = c^\dagger$. In the pole-zero controller form from (4), all tunings in Region 3 have purely real controller zeros, i.e., $\omega_{z1}, \omega_{z2} \in \mathbb{R}$. Furthermore, the controller zeros are placed on either side of the plant unstable pole ω_0, i.e., $\omega_{z1} < \omega_0 < \omega_{z2}$. Region 4 is characterized by the closed-loop poles d and e being the complex conjugate pair, i.e., the three fastest poles are purely real: $[a, b, c] \in \mathbb{R}$. In other words, as sorted, $d = d_r + jd_i$ and $e = d^\dagger$. Traversing Region 4 from lower to higher phase margin, the poles d and e migrate towards the imaginary axis. In the region with highest phase margin— approximating where $\phi_{PM} > 60°$—the complex conjugate poles dominate and induce excessive oscillations in the system response, even though phase margin is maximized. This counters the common intuition that higher phase margin results in a more damped response and is always better.

4.3.3   Regions 5 and 6—all real closed-loop poles

Region 5 is split in two sub-regions based on complex conjugate or purely real zeros. Traversing Region 5 from higher to lower phase margin, the zeros start as purely real and enclose the slowest closed-loop pole e and the plant unstable pole ω_0, i.e., $\omega_{z1} < |e| < \omega_{z2}$, $\omega_{z1} < \omega_0 < \omega_{z2}$. Traversing from the region limit of approximately $\phi_{PM} = 44°$ to $\phi_{PM} = 41°$, the controller zeros come together and converge at $\omega_{z1} = \omega_{z2} = \omega_0 = |e|$. Then, continuing to traverse from $\phi_{PM} = 41°$ to the region limit of approximately $\phi_{PM} = 38°$, the zeros split off axis. With complex conjugate zeros, the closed-loop poles are all faster than the real part of the zeros, i.e., $|a| > \ldots > |e| > \Re(\omega_{z1}) = \Re(\omega_{z2})$. This is the only region with complex zeros and no pole/zero cancellation occurs. Region 6 is characterized by the controller zeros—in the pole-zero controller form from (4)—being both purely real and both slower than the plant unstable pole ω_0, i.e., $\omega_{z1} < \omega_{z2} < \omega_0$. Furthermore, the controller zeros are set where the slowest two closed-loop poles are sandwiched between the zeros, i.e., $\omega_{z1} < |d| < |e| < \omega_{z2}$.

5   Conclusion

This paper investigates analytical tuning for magnetic levitation PID controllers using either pole placement or frequency design methods. Pareto optimal tunings are identified based on three system performance metrics. Overall, Fig. 3c presents the range of possible system responses given Pareto optimal tunings with the goal of users understanding the tuning design space. Users select the desired Pareto optimal tuning based on Figs. 3 and 4, depending on the desired bandwidth (control effort as dynamic stiffness) and robustness to uncertainty (unmodeled dynamics and/or parameter error). The tuning region is identified from Fig. 3 and Table 1 gives example controller parameters. The evolution of the pole-zero controller formulation is presented in Fig. 4 for how to select the controller zeros, pole frequency limits, and phase margin given the desired control bandwidth.

References

Anantachaisilp, P., Lin, Z. & Allaire, P. (2012), Pid tuning methods for active magnetic bearing systems, *in* '13th International Symposium on Magnetic Bearings'.

Bleuler, H., Jeon, J. & Higuchi, T. (1994), Self-tuning control for magnetic bearings, *in* '4th Int. Symp. on Mag. Bearings'.

Brunet, M. & Rioland, J. (1990), Self-tuning digital state controller for active magnetic bearings, *in* '2nd International Symposium on Magnetic Bearings'.

Chiba, A., Fukao, T., Ichikawa, O., Oshima, M., Takemoto, M. & Dorrell, D. (2005), *Magnetic Bearings and Bearingless Drives*, Newnes.

Maslen, E., Schweitzer, G., Bleuler, H., Cole, M., Keogh, P., Larsonneur, R., Nordmann, R., Okada, Y. & Traxler, A. (2009), *Magnetic Bearings—Theory, Design and Application to Rotating Machinery*, Springer Berlin Heidelberg.

Sawicki, J. & Maslen, E. (2008), Toward automated amb controller tuning: Progress in identification and synthesis, *in* '11th Int. Symposium on Magnetic Bearings'.

Yoon, S. Y., Lin, Z. & Allaire, P. (2012), Iterative tuning of linear quadratic controller for ambs in a high speed compressor, *in* '13th International Symposium on Magnetic Bearings'.